pK_a Measurements from Nuclear Magnetic Resonance for the B1 and B2 Immunoglobulin G-Binding Domains of Protein G: Comparison with Calculated Values for Nuclear Magnetic Resonance and X-ray Structures[†]

Devesh Khare,[‡] Patrick Alexander,[‡] Jan Antosiewicz,[§] Philip Bryan,[‡] Michael Gilson,[‡] and John Orban*[,‡]

Center for Advanced Research in Biotechnology, University of Maryland Biotechnology Institute, 9600 Gudelsky Drive, Rockville, Maryland 20850, and Department of Biophysics, University of Warsaw, 02-089, Warsaw, Poland

Received December 17, 1996; Revised Manuscript Received January 24, 1997[⊗]

ABSTRACT: Two-dimensional homo- and heteronuclear nuclear magnetic resonance (NMR) spectroscopy was used to determine pK_a values for all of the acidic residues in the B1 and B2 immunoglobulin G- (IgG-) binding domains of protein G. Due to the stability of protein G over a wide pH range, estimates of ionization constants were also obtained for some basic residues. These experimentally determined ionization constants were compared with values calculated from both X-ray and NMR-derived structures of B1 and B2 using the UHBD algorithm [Antosiewicz, J., et al. (1994) *J. Mol. Biol. 238*, 415−436]. This algorithm has been found to be predictive for pK_a measurements in proteins and, in combination with experimental measurements, allowed some evaluation of the NMR and X-ray structures. Three regions where significant differences exist between the X-ray and NMR structures are (1) the position of the E56 side chain relative to the backbone amides of K10 and D40, (2) residues 33−37 in the helix, and (3) the Y45 side-chain conformation. For all three cases, the experimental pH titration curves are notably more consistent with the X-ray structures than the NMR structures. In contrast, a number of solvent-accessible side chains have experimental pK_as more in agreement with mean pK_as calculated from families of NMR structures. The conformations of these side chains may be susceptible to crystal packing effects. From titration experiments under basic conditions, it is noteworthy that the chemical shift of the Y45 $C_\epsilon H$ resonance is invariant up to pD_{corr} 12. The Y45 side-chain hydroxyl group appears to maintain a nativelike hydrogen bond with D47 at pD_{corr} 12, even though the protein is approximately 90% unfolded. These results suggest that this short-range (i, $i + 2$) interaction, located in the $\beta3-\beta4$ hairpin, is present in the high-pH denatured state and may therefore form early in the folding of protein G.

The measurement of ionization constants in proteins using NMR spectroscopy is well-established (Cohen et al., 1973; Patel et al., 1975; Jardetzky & Roberts, 1981) and continues to be an important technique in characterizing electrostatic interactions. Recent examples include the study of ionization equilibria in thioredoxin (Forman-Kay et al., 1992; Jeng et al., 1995; Wilson et al., 1995 ; Jeng & Dyson, 1996; Qin et al., 1996), desulfatohirudin (Szyperski et al., 1994), turkey ovomucoid third domain (Schaller & Robertson, 1995), four lysozymes (Takahashi et al., 1992; Anderson et al., 1993; Bartik et al., 1994), myoglobin (Bashford et al., 1993), and HIV-1 protease (Wang et al., 1996). Complementary to these experimental measurements, a number of computational algorithms have been developed to calculate pK_a values of titratable groups in proteins, as reviewed elsewhere (Gilson, 1997). The programs require a detailed knowledge of the three-dimensional structure, derived from either X-ray crystallography or NMR spectroscopy. It is found empirically that the best statistical agreement with experiment is obtained when the protein interior is assigned a dielectric constant of 20 (Antosiewicz et al., 1994). Thus, in two recent studies, root-mean-square deviations from experiment of about 0.8 were found for over 60 groups in 8 globular proteins (Antosiewicz et al., 1994, 1996). Larger errors tend to be associated with groups that are sequestered from the solvent (Antosiewicz et al., 1994). It is not clear at this time whether the protein dielectric constant of 20 represents a realistic value or an unrealistic value that compensates for some other unrealistic feature of the electrostatics model, such as the use of a single conformation of the protein (Antosiewicz et al., 1994, 1996).

In this paper, we describe pK_a measurements for the B1 and B2 immunoglobulin G- (IgG-) binding domains of multidomain streptococcal protein G using NMR spectroscopy. Both domains are small 56 amino acid folding units that differ in sequence by six residues and bind tightly to the constant Fc region of IgG (Myhre & Kronvall, 1977; Reis et al., 1984; Fahnestock et al., 1986; Tashiro & Montelione, 1995). The B1 and B2 domains have high thermal stability with denaturation temperatures of 87.5 and 79.4 °C, respectively, at pH 5.4 (Alexander et al., 1992a). These domains are also stable or significantly folded over a wide pH range from approximately pH 1.5 to 11.6 at room temperature (Alexander et al., 1992b). This allows pK_a values to be obtained for some basic residues such as tyrosines and lysines as well as the more usual measurements for acidic groups. There are no histidine residues in either

[†] Supported by NSF Grant MCB-92-19309.

* Author to whom correspondence should be addressed.

[‡] Center for Advanced Research in Biotechnology, University of Maryland Biotechnology Institute.

[§] University of Warsaw.

[⊗] Abstract published in *Advance ACS Abstracts,* March 15, 1997.

S0006-2960(96)03092-9 CCC: $14.00

Table 1: Structures Used in This pK_a Study[a]

PDB ID	domain	method	no. of conformations in file	resolution/RMSD[b] (Å)
1PGA[c]	B1	X-ray	1	2.04
1PGB[c]	B1	X-ray	1	1.86
1GB1[d]	B1	NMR	60	0.27 ± 0.03/0.65 ± 0.05
1PGX[e]	B2	X-ray	1	1.67
1IGD[f]	B2	X-ray	1	1.1
2IGH[g]	B2	NMR	24	0.9 ± 0.2/1.9 ± 0.2

[a] The numbering system used here is the same as in Gallagher et al. (1994) and Gronenborn et al. (1991). This numbering is 13 less than that used by Achari et al. (1992) and 5 less than that used by both Lian et al. (1992) and Derrick and Wigley (1994). [b] Root mean square deviation of atoms about the average coordinate positions for backbone atoms/all atoms. [c] Gallagher et al. (1994). [d] Gronenborn et al. (1991). [e] Achari et al. (1992). [f] Derrick and Wigley (1994). [g] Lian et al. (1992).

B1 or B2. Also, the small size of protein G permits NMR spectra to be analyzed readily. Almost all the pertinent resonances of titratable groups are well-resolved in two-dimensional spectra acquired over the pH range used, providing well-determined titration curves.

The experimental pK_a values obtained here are compared with ionization constants calculated from an abundance of structural data on both domains using the UHBD algorithm (Davis et al., 1991). In this way, both the structures and the calculation process itself were assessed for their level of agreement with the experimental pK_a data. For the B1 domain, an NMR structure (Gronenborn et al., 1991) and two X-ray structures of orthorhombic and trigonal crystal forms (Gallagher et al., 1994) were used to calculate ionization constants. Similarly, one NMR structure (Lian et al., 1992) and two X-ray structures (Achari et al., 1992; Derrick & Wigley, 1994) were used for the B2 calculations. Structural data are summarized in Table 1.

There are three regions in protein G where the experimental pH titration curves are notably more consistent with the X-ray structures than the NMR structures. In contrast, a number of solvent-accessible side chains have pK_as more in agreement with the NMR structures. The titration experiments also provide some insights into the pH-dependent folding and stability of protein G.

MATERIALS AND METHODS

Sample Preparation. Unlabeled and ^{15}N-labeled protein G samples were cloned, expressed, and purified as described previously (Alexander et al., 1992a; Orban et al., 1995). A protein concentration of 3.4 mM was used for both B1 and B2 domains. Samples were dissolved in 0.45 mL of 90% H_2O/10% D_2O or 100% D_2O containing 100 mM sodium acetate-d_3 and the pH was adjusted by the addition of small amounts (1−2 μL) of concentrated HCl or NaOH solutions.

NMR Spectroscopy. NMR spectra were recorded on a Bruker AMX-500 and processed on Silicon Graphics workstations using FELIX (Molecular Simulations, Inc.). All spectra were acquired at 25 °C. Amide ^{1}H and ^{15}N chemical shifts were obtained from ^{1}H−^{15}N heteronuclear single quantum coherence (HSQC; Bodenhausen & Ruben, 1980; Bax et al., 1990; Norwood et al., 1990) spectra acquired in time-proportional phase incrementation (TPPI; Marion & Wuthrich, 1983) mode with no phase cycling (Marion et al., 1989). ^{15}N-Decoupling during t_2 was achieved using a GARP sequence (Shaka et al., 1985). The $1/(4J_{NH})$ delay was set to 2.3 ms, and the relaxation delay was 1.0 s. Spectral widths of 5000 and 1670 Hz were used in the ^{1}H and ^{15}N dimensions, respectively, and 1024 t_1 increments of 2K data points were used with 1 transient/increment. The final digital resolution was 0.005 ppm/point in the ^{1}H dimension and 0.016 ppm/point in the ^{15}N dimension. ^{1}H−^{15}N HSQC experiments were acquired in approximately 24 min. Solvent suppression was carried out using presaturation.

Homonuclear TOCSY (total correlation spectroscopy; Braunschweiler & Ernst, 1983) experiments were collected using natural-abundance samples and the above solution conditions. Spectra were acquired in TPPI mode with minimal phase cycling (Marion et al., 1989; Bax, 1989) using a DIPSI-2 (Shaka et al., 1988; Rucker & Shaka, 1989) mixing sequence and 1.0-ms trim pulses. The mixing time was 60 ms, and 512 t_1 increments of 2K data points were used with 2 transients/increment. The total data collection time at each pH was 22 min. Rapid acquisition was particularly important at high pH values (>11) where protein samples were not stable for extended periods. The digital resolution in both dimensions was approximately 0.006 ppm/point. Presaturation was used to suppress the residual water signal.

pH-Dependent Chemical Shift Measurements. The pH was measured before and after each spectrum was recorded. The latter reading was used in data analysis although the readings did not vary by more than 0.1 pH unit. The pH meter was calibrated prior to use with pH 4.00, 7.00, and 10.00 standard solutions. The estimated uncertainty in pH measurement is 0.02 pH unit. In D_2O solutions, meter readings were corrected for the isotope effect, where $pD_{corr} = pD_{read} + 0.4$ (Glasoe & Long, 1960; Bai et al., 1993). This only affects ionization constants for basic residues.

^{1}H−^{15}N HSQC spectra were collected at about 0.3 pH unit intervals between pH 1.5 and 7.0. The pH titrations of carboxylate groups were done starting at pH 7.0 and adjusting to lower pHs with acid. These samples were also titrated from pH 1.5 back to 7.0 at approximately 0.5−1 pH unit intervals and the ionization process was found to be completely reversible. In all, measurements were made at 22−23 different pH values between pH 1.5 and 7.0 for ^{15}N-labeled B1 and B2.

Homonuclear TOCSY experiments were recorded in a similar fashion with 22 measurements between pH 7.0 and 1.5 and a further 14−16 spectra acquired between pD_{corr} 8.4 and 12.0. Measurements made below pH 7.5 were done in 90% H_2O/10% D_2O solutions and high pH measurements were done in 100% D_2O solutions. Chemical shifts were calibrated using TSP (sodium 3-trimethylsilylpropionate; Cambridge Isotope Laboratories) as an external reference. The chemical shift of the water signal with respect to TSP varied only slightly with pH. The largest change in chemical shift (0.02 ppm) occurred between pH 4and 6 and measurements in this range were corrected appropriately. There was negligible change (<0.005 ppm) above pH 6. These results are consistent with previous observations (Forman-Kay et al., 1992) as well as values obtained from the empirical relationship between pH and TSP chemical shift (DeMarco, 1977; Bundi & Wuthrich, 1979).

Determination of Apparent pK_a Values from Experimental Data. pK_a values were obtained from nonlinear fits of the

titration data to eq 1, derived from the Henderson−Hasselbalch equation:

$$\delta_{obs} = (\delta_{HA} + \delta_{A^-}10^{pH-pK})/(1 + 10^{pH-pK}) \quad (1)$$

where δ_{obs} is the observed experimental chemical shift, δ_{HA} is the chemical shift of the protonated group, and δ_{A^-} is the chemical shift of the deprotonated group. The curve fitting was carried out on a MacIntosh Classic using KaleidaGraph version 3.0.2 (Abelbeck Software).

Calculation of pK_a Values from X-ray and NMR Structures. The computational methods used here have been described previously (Antosiewicz et al., 1994, 1996). Briefly, the pK_a of an ionizable group is defined as the pH for which it is half-ionized. The charge states are computed with an algorithm (Gilson, 1993) that is based upon statistical thermodynamic theory described elsewhere (Schellman, 1975; Bashford & Karplus, 1990; Gilson, 1993). This theory requires as input the interaction energies among the ionizable groups of the protein and the difference between the energy of ionizing each group in the otherwise neutral protein, relative to the energy of ionizing it in bulk solvent. These energies are all assumed to be electrostatic in nature, and are computed by the Poisson−Boltzmann model (Warwicker & Watson, 1982; Gilson et al., 1985, 1988; Klapper et al., 1986; Gilson & Honig, 1988; Honig et al., 1993; Madura et al., 1994). These energy calculations, in turn, take as inputs the structure of the protein and a number of other parameters. The inputs are described next.

When a group ionizes, its net charge and its charge distribution both change. Here, the charge change upon ionization is modeled in a simple way that has been shown to be predictive for about 60 measured pK_as (Antosiewicz et al., 1994). In this approach, the full set of partial atomic charges appropriate to the neutral state of each group is taken as the starting point. Ionization is then modeled as the addition or subtraction of a unit charge at one atom of the group. The atomic charges and radii used with this model are the same as those used previously (Antosiewicz et al., 1994): the charges are based upon the CHARMm version 22.0 atomic parameters that include only polar hydrogens (Molecular Simulations Inc., Waltham, MA., 1992), and the radii are based upon the OPLS nonbonded parameter set (Jorgensen & Tirado-Rives, 1988).

Before the electrostatics calculations can be carried out, coordinates must be established for hydrogens. As discussed previously (Antosiewicz et al., 1996), hydrogen coordinates are calculated for X-ray and NMR structures by the same procedure. First, rotational orientations are assigned to carboxylic acids. The default is to place the proton on the oxygen that occurs second in the file of atomic coordinates. For the C-termini of peptides, the proton is linked to the OXT atom in the neutral form. Once these assignments have been made, the HBUILD (Brunger & Karplus, 1988) command of CHARMm version 23.1 (Brooks et al., 1983) is used to establish energetically reasonable hydrogen positions. Finally, the energy of the system is minimized with respect to the positions of the hydrogens only by 500 steps of steepest descent energy minimization with CHARMm.

The dielectric constant of the aqueous solvent is set to 78 and that of the protein to 20 (Antosiewicz et al., 1994). The ionic strength of the solvent is set to 100 mM, and the Stern layer is 2 Å thick.

The atomic coordinates of the streptococcal protein G domains used for the calculations are drawn from the Protein Data Bank (Bernstein et al., 1977). The coordinate sets are identified in Table 1. Each NMR file contains multiple conformations of the same protein. Therefore, separate pK_a calculations were executed for each conformation, and the resulting pK_as were averaged. In addition, the root-mean-square deviation from the mean was calculated as an index of the variation of the computed pK_as among the various conformations.

Modeling Studies. Quanta and CHARMm (Molecular Simulations Inc., Waltham, MA) were used with the CHARMm 22.0 all-hydrogen force field in modeling studies of the Q32−D36 interaction. Calculations were done with a fixed dielectric constant of 1. Similar results were obtained when some of the calculations were repeated with the distance-dependent dielectric option. Energy minimizations used 500 steps of the conjugate gradient algorithm. These appeared to be well converged, from inspection of the rate of change of energies and key interatomic distances.

RESULTS

Complete assignments were made previously for ^{1}H and ^{15}N resonances at pH 3.0 and 5.4 for the B1 and B2 IgG-binding domains of protein G (Orban et al., 1992, 1995). Using these assignments, in combination with chemical shift measurements over approximately 40 different pH values from pH 1.5 to 12.0, made resonance assignment at different pH values straightforward. Main-chain and side-chain amide proton and nitrogen chemical shifts were obtained from ^{1}H−^{15}N HSQC experiments, while side-chain proton chemical shifts were from homonuclear TOCSY experiments. Experimentally determined ionization constants were compared with calculated values for NMR and X-ray structures of B1 and B2 and the results are summarized in Table 2. A number of ionization constants deviate from intrinsic values (Tanford & Kirkwood, 1957; Honig & Hubbell, 1984; States & Karplus, 1987), indicating the presence of hydrogen bonds or salt bridges.

Aspartate and Glutamate Residues. Titration curves were obtained for all aspartate and glutamate residues in the B1 and B2 domains. The B1 domain contains five aspartates (D22, D36, D40, D46, and D47) and five glutamates (E15, E19, E27, E42, and E56), whereas B2 has four glutamates (E15, E24, E27, and E56) and five aspartates (as above). Titration shifts ($\Delta\delta = \delta_{A^-} - \delta_{HA}$) of >0.05 ppm for ^{1}H data and >0.5 ppm for ^{15}N data were considered to be significant over the pH range 1.5−7.0. Experimental ionization constants reported for aspartate residues are an average of the pK_a values obtained from individual pH-titration curves for the C_βH and C_βH′ protons and backbone amide nitrogens. For the glutamate residues, pK_as are from C_γH/C_γH′ proton and backbone amide nitrogen titration curves. In cases where a carboxylate group H-bonds to an amide, the pK_a obtained from the amide is also included in the averaging (see Table 2 legend). Backbone amide protons with titration shifts less than 0.1 ppm were not used to obtain pK_a values.

Side-chain C_βH resonances provided pH-dependent changes in ^{1}H chemical shifts of $\Delta\delta \sim 0.1-0.3$ ppm for aspartate residues while the C_γH resonances were the most sensitive side-chain protons for glutamate residues ($\Delta\delta \sim 0.2-0.3$ ppm). Proton chemical shift titration curves for B2 are

Table 2: Calculated and Experimental pK_a Values for B1 and B2 at 25 °C

	B1					B2				
	NMR[a]		X-ray			NMR[a]		X-ray		
residue	mean	RMSD	1PGA	1PGB	exp[b]	mean	RMSD	1IGD	1PGX	exp[b]
Y3	13.1	0.7	12.4	12.2	>11	13.1	0.4	11.3	11.9	>11
K4	11.3	0.3	11.5	12.2	>11	10.7	0.5	11.5	10.7	~11
K10	11.2	0.3	11.5	11.3	~11	11.3	0.6	11.5	10.8	>11
K13	11.1	0.2	11.4	11.4	>11	10.9	0.4	10.9	10.7	>11
E15	3.9	0.4	3.5	2.3	4.4 ± 0.1	4.0	0.5	3.9	4.2	4.3 ± 0.15
E19K	4.2	0.1	4.1	4.2	3.7 ± 0.15	10.4	0.4	10.5	10.6	10.7
D22	2.9	0.2	3.0	3.3	2.9 ± 0.1	3.5	0.4	3.0	3.3	2.9 ± 0.2
A24E						4.2	0.4	3.9	4.6	4.2 ± 0.1
E27	4.4	0.2	2.3	3.3	4.5 ± 0.1	4.2	0.6	3.5	3.2	4.6 ± 0.1
K28	10.6	0.2	12.1	10.4	10.9	10.9	0.4	11.8	11.6	~11
K31	11.5	0.2	10.6	11.4	nd[c]	11.4	0.5	11.6	11.2	nd[c]
Y33	10.2	0.1	10.5	10.7	~11	10.3	0.5	10.4	10.4	~11
D36	4.2	0.2	4.4	4.3	3.8 ± 0.1	4.1	0.1	4.1	4.7	3.9 ± 0.1
D40	4.1	0.3	4.1	4.4	4.0 ± 0.2	4.2	0.8	4.1	4.0	4.0 ± 0.2
E42V	4.8	0.4	4.7	4.8	4.4 ± 0.1					
Y45	12.5	0.5	14.6	14.7	>12	11.3	0.5	14.6	15.0	>12
D46	4.0	0.1	4.0	4.1	3.6 ± 0.1	3.1	0.4	4.0	3.6	3.6 ± 0.1
D47	3.6	0.2	2.7	3.1	3.4 ± 0.3	3.8	0.5	2.7	3.2	3.4 ± 0.3
K50	11.0	0.3	12.2	12.3	nd[c]	11.1	0.5	12.4	12.2	nd[c]
E56	5.7	0.5	4.1	4.0	4.0 ± 0.1	5.5	0.5	4.5	4.4	4.2 ± 0.1

[a] Calculations for NMR structures were done for each conformer in the PDB file and then averaged to provide a mean pK_a and root mean square deviation for each ionizable group. [b] For aspartates, experimental ionization constants are an average of apparent pK_a values from C_βH, C_βH′, and backbone ^{15}N titration curves. In cases where aspartates are involved in H-bonds to main-chain or side-chain amides (see text), the relevant amide titration curves were also used in the average. For D40, only the apparent pK_as from C_βH and C_βH′ were used to obtain an average pK_a. For glutamates, C_γH, C_γH′, and backbone ^{15}N resonances were used except for E56. In this case, the apparent pK_a from E56 C_γH was used in conjunction with apparent pK_as for K10 and D40 backbone amide ^{1}H and ^{15}N titration curves to obtain the average pK_a. Errors are reported at 1 standard deviation. For tyrosine and lysine residues, ionization constants were determined from C_ϵH titration curves. [c] Not determined due to resonance overlap.

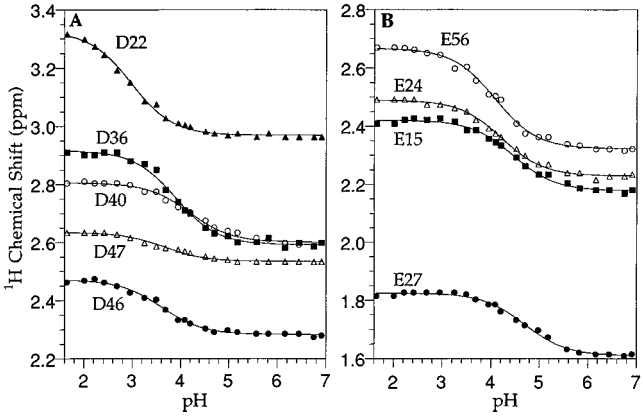

FIGURE 1: pH dependence of ^{1}H chemical shifts in the B2 domain for (A) C_βH′ resonances of aspartate residues D22 (filled triangles), D36 (filled squares), D40 (open circles), D46 (filled circles), and D47 (open triangles) and (B) C_γH resonances of E15 (filled squares), E24 (open triangles), E27 (filled circles), and E56 (open circles). Solid lines represent fits to eq 1. Chemical shifts are from homonuclear TOCSY spectra recorded at 25 °C.

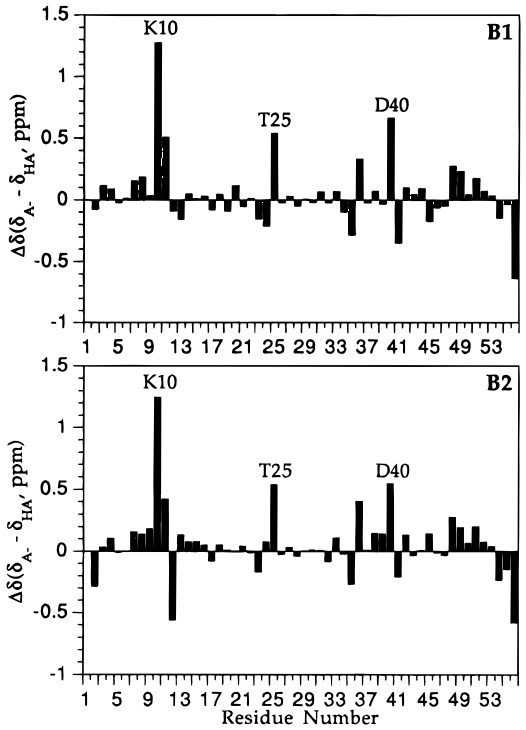

FIGURE 2: Titration shifts ($\Delta\delta$) for main-chain amide protons in the B1 and B2 domains where δ_{HA} is the chemical shift at pH 1.6 and δ_{A^-} is the shift at pH 7.0.

shown in Figure 1. Comparable curves were obtained for the B1 domain. The pH-dependent changes in ^{1}H chemical shifts of C_αH and main-chain NH resonances were typically smaller with $\Delta\delta$ < 0.2 ppm. Titration shifts were also obtained for 55 main-chain amide protons and nitrogens from ^{1}H−^{15}N HSQC data in the pH range 1.5−7.0. The ^{1}H data are summarized in Figure 2 for both domains. A number of residues, including K10, T25, and D40 displayed relatively large changes in their main-chain amide proton and nitrogen chemical shifts with $\Delta\delta \geq 0.5$ ppm for ^{1}H and $\Delta\delta \geq 3$ ppm for ^{15}N.

The pH dependence of side-chain amide proton and nitrogen chemical shifts was also monitored for all residues containing primary amide groups (N8, Q32, N35, and N37). Only Q32 displayed significant changes in ^{1}H (0.6 ppm) and ^{15}N (3 ppm) chemical shifts with pH. Interestingly, the H_E proton shift showed sigmoidal pH-dependent behavior while the H_Z proton shift was relatively insensitive to pH change ($\Delta\delta \sim 0.05$ ppm). Assignment of the H_E and H_Z protons

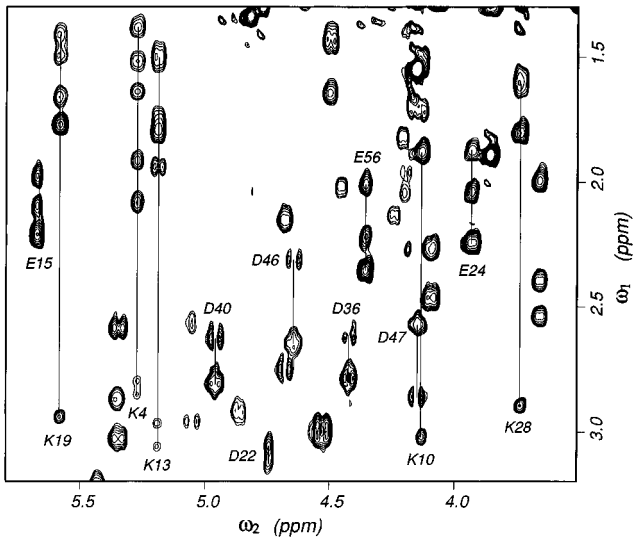

FIGURE 3: Part of the $C_\alpha H$ to side-chain region of the D_2O TOCSY spectrum (τ_m 60 ms) for B2 showing side-chain assignments for aspartate, glutamate, and lysine residues at 25 °C, pD_{corr} 10.

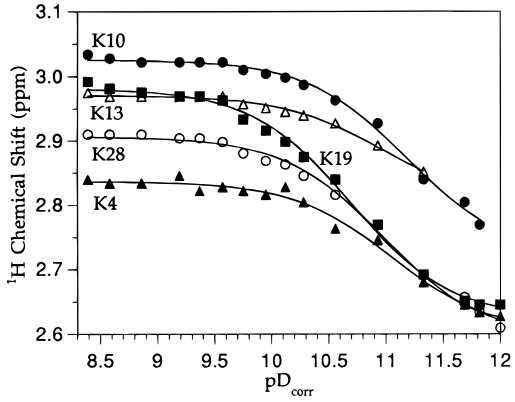

FIGURE 4: pD_{corr} dependence of proton chemical shifts for lysine $C_\epsilon H$ resonances in the B2 domain. Residues are represented as follows: K4 (filled triangles), K10 (filled circles), K13 (open triangles), K19 (filled squares), and K28 (open circles). Solid lines show fits to eq 1.

was unambiguous since the H_E proton has a more intense NOE to Q32 $C_\gamma H$ than H_Z does. Our assignment is also consistent with the general observation that the H_E resonance is further downfield than the H_Z resonance (Redfield & Waelder, 1979; Perrin & Arrhenius, 1982).

Lysine Residues. Reasonable titration curves up to pD_{corr} 12 were obtained by monitoring the lysine $C_\epsilon H$ chemical shifts using TOCSY spectra acquired in D_2O. Figure 3 shows the level of resolution obtained from these spectra for assignment of side-chain resonances. The $C_\epsilon H$ protons were found to be the most sensitive to change in pH due to their proximity to the titrating ϵ-ammonium group. Typical titration shifts ($\Delta\delta = \delta_A - \delta_{HA^+}$) were in the -0.20 to -0.35 ppm range. In B1, four out of six $C_\epsilon H$ shifts can be readily observed and in B2 five of seven are easily detectable. Reliable titration curves could not be obtained for K31 and K50 in either domain due to overlap in the TOCSY spectra. Only lower limits of ionization constants were determined for some lysine residues since reliable chemical shifts could not be obtained at the high pD part of the curves due to extensive protein denaturation (Table 2; Figure 4).

Tyrosine Residues. The proton chemical shifts of the three tyrosine residues in B1 and B2 were assigned previously

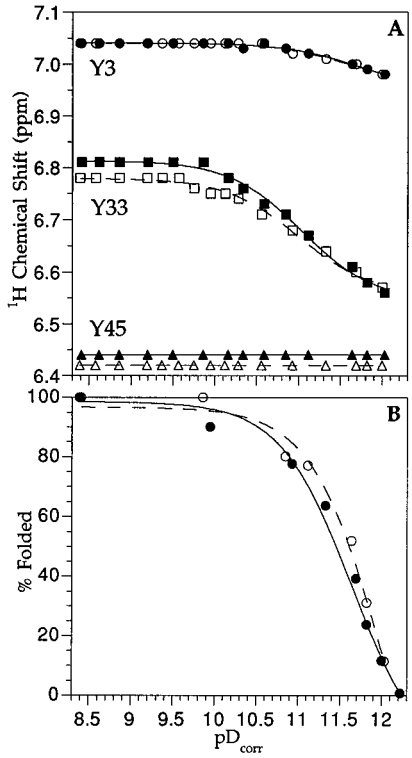

FIGURE 5: (A) Chemical shift versus pD_{corr} plots for tyrosine $C_\epsilon H$ resonances in the B1 (filled symbols, solid lines) and B2 (open symbols, broken lines) domains of protein G. Residues are represented as follows: Y3 (circles), Y33 (squares), and Y45 (triangles). (B) Percent folded protein versus pD_{corr} for B1 (open circles, broken line) and B2 (filled circles, solid line) from normalized integrals of the V54 γ-methyl resonance as a function of pH.

(Gronenborn et al., 1991; Lian et al., 1992; Orban et al., 1992). Proton chemical shifts of the aromatic $C_\delta H$ and $C_\epsilon H$ resonances were readily monitored as a function of pH from TOCSY spectra recorded in D_2O. The signal due to $C_\epsilon H$ was more sensitive to changes in pH than the $C_\delta H$ signal, consistent with its proximity to the titratable $O_\eta H$ group. Experimental and calculated ionization constants for tyrosine residues are summarized in Table 2. Tyrosine titration curves and the high-pH denaturation profiles are shown for B1 and B2 in Figure 5. An ionization constant was estimated for Y33 although the high-pH side of the curve was incomplete due to significant denaturation. Only lower limit pK_a values could be estimated for Y3 and Y45. The denaturation profile at high pH was determined in D_2O by integrating the upfield-shifted γ-methyl resonance of V54, a diagnostic peak for folded protein, as a function of pD_{corr}. The results shown in Figure 5B are consistent with data obtained from CD (Alexander et al., 1992b) and quenched-flow experiments (Alexander et al., unpublished results).

DISCUSSION

Hydrogen-Bonding Interactions between Side Chains and the Backbone. The large titration shifts of a number of main-chain NHs, particularly K10, T25, and D40 (Figure 2), indicate that these residues are involved in H-bonds with side-chain carboxylate groups [cf. Bundi and Wuthrich (1979), Ebina and Wuthrich (1984), and Szyperski et al. (1994)]. The pK_a values obtained from titration of these backbone amide protons and nitrogens correspond closely with ionization constants obtained for the interacting side

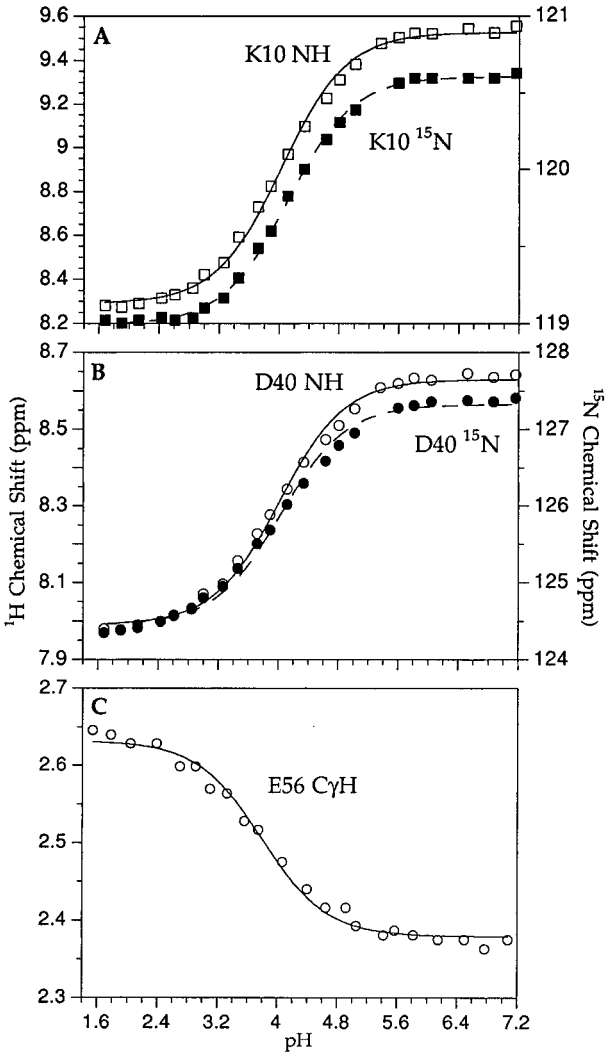

FIGURE 6: Chemical shift versus pH plots for (A) the backbone amide proton (open squares, solid line) and nitrogen (filled squares, broken line) of K10; (B) the backbone amide proton (open circles, solid line) and nitrogen (filled circles, broken line) of D40; and (C) the $C_\gamma H$ resonance of E56. Titration curves shown are for the B1 domain.

chains. Figure 6 shows the titration curves for the backbone amides of K10 and D40 as well as the $C_\gamma H$ group of E56. The pK_a values obtained from all three sets of curves are very similar and suggest that the proximal E56 side-chain carboxylate H-bonds to both K10 and D40 backbone NHs. The experimental pK_a values for the E56 side-chain carboxylate are consistent with ionization constants calculated from the X-ray structures of B1 and B2 but are 1.3−1.7 units lower than the pK_as calculated from the NMR structures (Table 2).

The discrepancy in calculated values for E56 is due to notable differences between the X-ray and NMR structures in this region. In the X-ray structures of B1 and B2, the E56 side-chain carboxylate has H-bonding interactions with the main-chain NHs of K10 and D40 (Figure 7). In the corresponding NMR structures, this H-bonding interaction is absent, with the E56 γ-carboxylate more than 6.0 Å on average from the backbone NHs of K10 and D40. The high pK_as calculated for the E56 γ-carboxylate in the NMR structures appear to be due to close contacts with either the C-terminal carboxylate in B1 or the β-carboxylate of D40 in B2. The B1 and B2 NMR structures were determined at

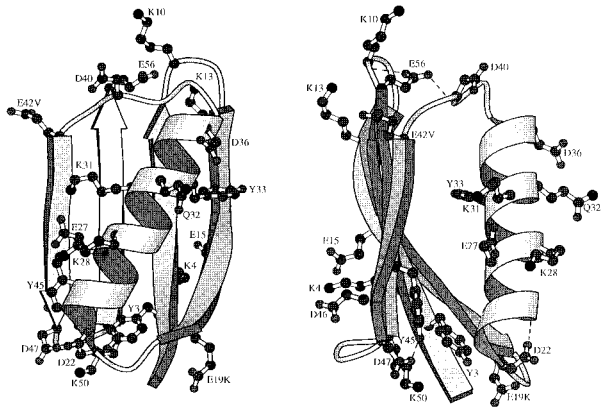

FIGURE 7: Two orthogonal views of the B1 X-ray structure, 1PGA (Gallagher et al., 1994), showing all the ionizable side chains in the protein plus Q32. The hydrogen bonds mentioned in the text involving residues E56−K10/D40, D22−T25, and Y45−D47 are shown as dashed lines. The figure was generated using MOLSCRIPT (Kraulis, 1991).

pH 4.34 and 4.2, respectively, while the X-ray structures were determined at pH 4.5 (1PGA), pH 4.0 (1PGB), pH 5.5 (1PGX), and pH 4.8 (1IGD). Based on the titration curves obtained here, the E56 side chain of B1 is about 65% in the carboxylate form at pH 4.34 while that of B2 is about 50% ionized at pH 4.2. Under these conditions, the K10−E56−D40 bifurcated H-bond network is only transiently populated, resulting in averaged NMR structures which do not reflect the H-bonding interactions. This exemplifies the high degree of sensitivity of the titration shift measurements in obtaining data on H-bonding interactions between backbone amides and side-chain carboxylates in solution. These types of interactions can frequently be missed using only NOE and coupling constant information (Wagner, 1990; Szyperski et al., 1994). Since the 1PGB crystal structure was determined under conditions where the E56 side chain is 50% ionized, it may be that the more ordered, H-bonded, structure crystallizes preferentially.

The H-bonding network between the fully deprotonated E56 side chain and the main-chain NHs of K10 and D40 appears to be quite well populated. Most significantly, the experimental ionization constants closely parallel the values calculated for the static X-ray structures rather than being in between the X-ray and NMR values as would be expected for a mixed population of conformers. In addition, the titration shifts are large, particularly for K10 where $\Delta\delta$ (^{1}H) is 1.3 ppm (Figure 2). A number of factors may influence titration shifts and the smaller $\Delta\delta$ of 0.7 ppm for D40 may be due to a poorer H-bond geometry with the E56 γ-carboxylate group as observed in the X-ray structures. Therefore, our results indicate that this stabilizing H-bonded network, bridging the $\beta1-\beta2$ turn and the helix−$\beta3$ loop, occurs in solution as well as in the crystal and may partly account for the sharp decrease in stability of the B1 domain below pH 3.5 (Alexander et al., 1992a).

The titration curves for the main-chain NH of T25 and the carboxylate of D22 are very similar (Figure 8), indicating that an H-bond exists between these two proximal moieties. There is reasonable agreement between experimentally determined ionization constants for D22 and those calculated from both X-ray and NMR structures (Table 2). All of these structures for B1 and B2 have the D22 carboxylate group within H-bonding distance of the main-chain amide of T25,

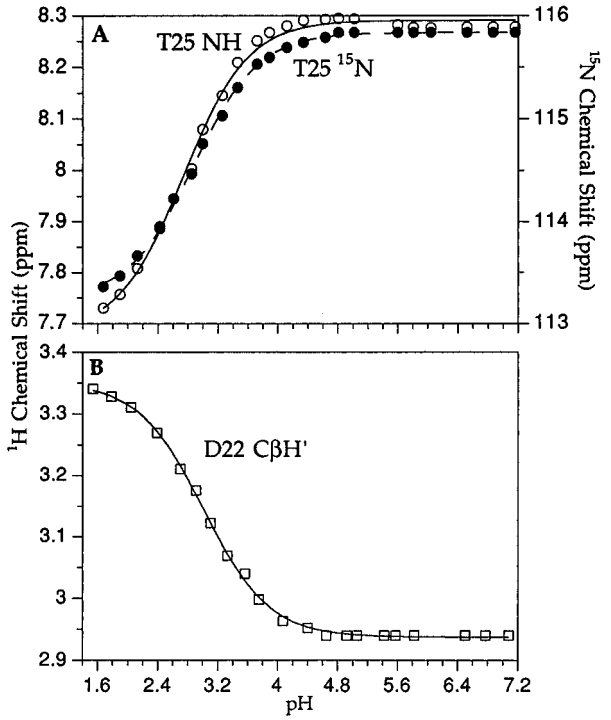

FIGURE 8: (A) pH dependence of the T25 backbone amide ^{1}H (open circles, solid line) and ^{15}N (filled circles, broken line) chemical shifts. (B) Titration curve for the $C_{\beta}H'$ resonance of D22. Both panels are for the B1 domain.

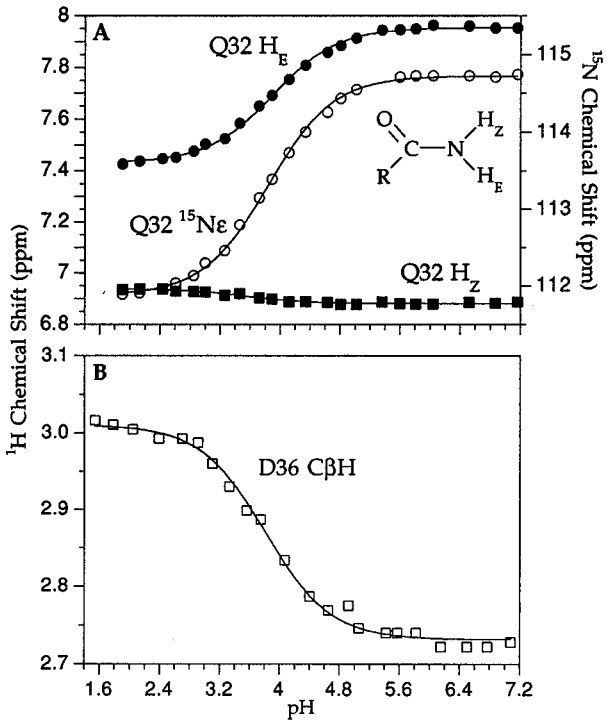

FIGURE 9: (A) Titration curves for the Q32 side-chain amide resonances in B1 at 25 °C, represented as follows: H_E proton (filled circles), H_Z proton (filled squares), and ϵ-nitrogen (open circles). Solid lines are fits of the data to eq 1. (B) Proton chemical shift versus pH plot for the $C_{\beta}H$ resonance of D36 in the B1 domain. Similar curves were obtained for the B2 domain.

forming a N-terminal cap on the helix. The low pK_a (2.9) obtained for D22 indicates that this stabilizing interaction persists to quite low pH values. This is generally consistent with the view of local stability in protein G since the N-terminal half of the helix is one of the more stable regions in the protein as determined from hydrogen exchange measurements (Orban et al., 1994, 1995).

Smaller titration shifts ($\Delta\delta \sim 0.3-0.5$ ppm) occur for the main-chain NHs of T11, D36, and A48 (Figure 2). The T11 shift is presumably due to its location next to the K10−E56 H-bond while the D36 shift is not well understood at present since intrinsic shifts of aspartate groups tend to be in the opposite direction (Bundi & Wuthrich, 1979). The shift for the backbone NH of A48 appears to be associated with titration of the carboxylate of D46 (data not shown). These two groups are within H-bonding distance in all of the protein G structures used in this study.

Structural Implications of the Hydrogen-Bonding Interaction between Q32 and D36 Side Chains. The pK_a values obtained experimentally for the D36 carboxylate correlate closely with the titration curve obtained for one of the primary amide protons in the Q32 side chain (Figure 9). Since D36 is the only acidic residue with spatial proximity to the Q32 side chain, these results indicate that the Q32 and D36 side chains are involved in a stabilizing H-bonded contact with each other. Only the H_E proton chemical shift of Q32 is significantly perturbed with pH whereas the H_Z proton shift is very small. Similar observations were made in a series of peptide fragments containing a glutamine to aspartate (i, $i + 4$) interaction (Huyghues-Despointes et al., 1995). The stereospecific interaction is found to be worth −1 kcal/mol of Gibbs free energy stabilization when the aspartate is deprotonated, as estimated from CD measurements. In the peptide fragment study, the change in ^{1}H chemical shift for the H_E glutamine resonance from pH 2 to 6 was 0.22 ppm. By comparison, the corresponding change in shift of Q32H_E in B1 and B2 is substantially larger (0.6 ppm) suggesting that the glutamine−aspartate (i, $i + 4$) H-bond in proteins may be even stronger or more populated than determined for short peptides. Indeed, a survey of the Protein Data Bank indicated that this (i, $i + 4$) arrangement is relatively common in helices of protein structures (Huyghues-Despointes et al., 1995).

With regard to the helix conformation, notable differences exist between the X-ray and NMR structures of B1 and B2. In the NMR structure of B1, residues 22−32 are α-helical while residues 33−37 are reported to form a 3_{10}-helix (Gronenborn et al., 1991). Additionally, a bound water molecule was reported at the α−3_{10} junction, between the carbonyl group of V29 and the amide proton of Y33 (Clore & Gronenborn, 1992). In another NMR study (Lian et al., 1992), the protein G B2 structures were found to contain α-helices from residues 23 to 35 and a slightly disordered C-terminal helical region from residues 36 to 38. By contrast, all of the X-ray structures of protein G domains used in this study show the helix as being entirely α-form from residues 23 to 38.

In an effort to resolve these discrepancies, we surveyed the relationship between the side chains of Q32 and D36 in the 60 NMR structures of B1. As noted above, the chemical shift data described here indicate an H-bond between Q32 H_E and a D36 O_{δ} but not between Q32 H_Z and a D36 O_{δ}. For an amide−carboxylate H-bond, the usual proton oxygen distance is 1.93 ± 0.16 Å (Taylor et al., 1984), and the usual O···H−N angle is 162°. None of the 60 NMR structures of B1 have the stereospecific H-bond between Q32 H_E and D36 O_{δ}. Model 36 shows the closest approach of either H_E or H_Z of Q32 to a carboxylate oxygen of D36: the H_E···$O_{\delta 1}$

distance and N−H_E···$O_{\delta 1}$ angle are 2.44 Å and 121°, respectively. The remaining models all have distances greater than about 3.5 Å for this interaction, with a distance of about 6 Å for the average structure. Thus, the Q32−D36 H-bond is not represented by the family of NMR structures. However, it is possible that this H-bond could be formed given minor changes in the NMR structures. This possibility was examined by a small computational study of model 36. First, energy minimization of an isolated glutamine−aspartate pair showed that the optimal proton-oxygen distance in the CHARMm force field is 2.06 Å, rather than the 1.93 Å obtained from analysis of small molecule crystal structures. Next, model 36 was energy-minimized with residues 32−36 mobile and all other atoms fixed. This led to a modest rearrangement that changed the shortest H_E···O_δ distance to 2.14 Å and the corresponding N−H_E···O_δ angle to 99.7°. In this conformation, Q32 H_Z was only 2.08 Å from D36 $O_{\delta 2}$, inconsistent with the absence of significant chemical shift change with pH for this proton. In order to force H_E close to a carboxylate oxygen but leave H_Z distant, an artificial restraint was used to bring H_E to 1.93 Å from D36 $O_{\delta 2}$ during a new energy minimization. Then the restraint was removed and the structure was allowed to relax to a new local energy minimum. This procedure placed H_E 2.14 Å away from each D36 O_δ, with an H-bond angle of 159°. It also left H_Z greater than 2.81 Å away from either D36 O_δ, consistent with the chemical shift results reported here. However, the procedure also led to some structural rearrangement of the backbone of residues 32−36 whereby the H-bond between Y33 and D36 was broken and a new (*i*, *i* + 4) H-bond formed between the main-chain carbonyl group of Q32 and the amide proton of D36, consistent with an α-helical arrangement. The backbone rearrangement seems to be important in establishing the proper relative conformation of Q32 and D36. Thus, when the procedure was repeated with only the side-chain and backbone atoms of residues 32 and 36 free to move, instead of all atoms of residues 32−36, it was not possible to establish a conformation in which H_E was near a D36 O_δ while H_Z was distant, as required by the data presented here.

The Q32 H_E−D36 O_δ interaction was also analyzed in the highest resolution crystal structure of B2, 1IGD. Here, the shortest Q32 H_E−D36 O_δ distance is 2.12 Å and the corresponding N−H_E···O_δ angle is 136°. The H_Z proton of Q32 is 3.62 Å from the nearest D36 O_δ, consistent with the interaction data presented here. Unrestrained energy minimization with only the side chains of residues 32 and 36 mobile yields a good H-bond between D36 $O_{\delta 2}$ and Q32 H_E, with an O···H distance of 2.08 Å and an O···H−N angle of 169°. This distance is very close to the optimum of 2.06 Å for this force field (see above). Moreover, the closest approach of Q32 H_Z to either D36 O_δ is 2.82 Å in the final conformation. Thus, the overall geometry is consistent with the chemical shift data presented here and is achieved with minimal adjustment of the crystal conformation. In particular, it is not necessary to change the α-helical backbone conformation of the residues between 32 and 36.

In summary, the 1IGD crystal conformation appears to agree better with the observed interactions between Q32 and D36 than does the B1 NMR structure. It has been observed previously that an H-bond from glutamine H_E to an aspartate O_δ four residues away (*i*, *i* + 4) is readily accommodated in an α-helix, as in the crystal structure (Huyghues-Despointes et al., 1995). It would appear that such an interaction is more difficult to establish in the 3_{10} helical structure found in the NMR study of B1.

Electrostatic Interactions between Glutamate and Lysine Residues. The glutamate residues at positions 19, 24, and 42 have experimental and calculated ionization constants that are within ± 0.4 unit for both X-ray and NMR structures (Table 2). This indicates that the average conformation of these surface side chains is adequately represented in both types of structure determination. In contrast, the calculated pK_a of the E56 γ-carboxylate differs significantly (1.3−1.7 units) between the NMR and X-ray structures due to differences in side-chain to backbone interactions as discussed above. Additionally, the experimental pK_as for E15 and E27 in B1 are 0.9−2.2 units higher than the values calculated from X-ray structures but are consistent with values derived from NMR structures. Smaller differences are observed in B2.

These differences can be rationalized by inspection of the relevant structures. In the B1 X-ray structures, the nearest E27 carboxylate oxygens are within 3.9 Å of the K28 ε-ammonium nitrogen and 3.0 Å of the K31 side-chain nitrogen atom. Electrostatic interactions between E27 and the side chains of K28 and K31 would have the effect of stabilizing the carboxylate moiety and therefore lowering its pK_a. This is reflected in the low pK_as calculated for E27 in the X-ray structures, particularly 1PGA. In contrast, the average NMR structure of B1 shows the nearest E27 carboxylate oxygens 9.9 and 8.5 Å from the side-chain nitrogen atoms of K28 and K31, respectively. Consequently, the mean pK_a of 4.4 ± 0.2 calculated from the NMR structure is significantly higher than for 1PGA or 1PGB and is in better agreement with the experimental value of 4.5 ± 0.1. Similarly, the low pK_a value calculated for E15 in 1PGB is due to a close contact with the K4 ε-ammonium group.

These results suggest that the K28−E27−K31 and E15−K4 stabilizing electrostatic interactions observed in the crystal forms are only transient in solution since the corresponding calculated pK_as in 1PGA and 1PGB are considerably lower than experimental values. The calculated pK_as of E15 and E27 are significantly different in the orthorhombic (1PGA) and trigonal (1PGB) crystal forms, suggesting that some of the observed differences may be partly due to crystal packing effects. Indeed, the largest differences in calculated pK_as between 1PGA and 1PGB are for E15, E27, K4, K28, and K31.

pH Titration of Tyrosine Residues. Implications for the Three-Dimensional Structure and Folding. Of the three tyrosine residues in protein G, only Y33 has a sufficiently low pK_a that it can be estimated from experimental data. The estimated pK_a is reasonably consistent with values calculated for both X-ray and NMR structures (Table 2). This ionization constant is not perturbed appreciably from its intrinsic value since the tyrosine side-chain hydroxyl group is solvent-exposed and does not appear to interact with other residues. Although the pK_as of Y3 and Y45 could not be determined, the order of the experimental pK_a values for the three tyrosine residues was established as Y45 > Y3 > Y33 for both B1 and B2 (Table 2, Figure 5A). This is consistent with the pattern of calculated tyrosine ionization constants for the X-ray structures but is not in agreement with the order of mean pK_a values calculated for NMR structures.

The pK_a values calculated for Y45 are quite different in the X-ray and NMR structures (Table 2). The Y45 ionization constants calculated for the X-ray structures of B1 and B2 are 2.1−3.7 pH units higher than the mean values calculated for the corresponding family of NMR structures. This discrepancy is due to a difference in the position of the Y45 side chain between the NMR and X-ray structures (Gallagher et al., 1994). In the NMR structure of B1, the hydroxyl proton of Y3 is H-bonded to the hydroxyl oxygen atom of Y45. This would stabilize the protonated form of Y3 and consequently leads to a higher calculated mean pK_a for Y3 (13.1) than Y45 (12.5). Similar ionization constants are calculated for the B2 solution structure (Table 2). However, the H-bonded interaction between Y3 and Y45 side chains does not exist in the X-ray structures of either B1 or B2. Instead, the hydroxyl proton of Y45 is 1.7 Å from the nearest carboxylate oxygen of D47 with an O−H···O angle of 175°. This, in turn, leads to a considerably higher calculated pK_a for Y45 than for Y3 in both domains, consistent with the experimental order of ionization constants. Therefore, if the calculated ionization constants are valid, our results imply that the solution conformation of the Y45 side chain is more accurately represented by the X-ray structures than the NMR structures.

It is noteworthy that Y45 shows no detectable change in its $C_\delta H$ or $C_\epsilon H$ chemical shifts up to pD_{corr} 12 (Figure 5A). This suggests that the Y45 side chain is still completely in the protonated form at pD_{corr} 12, apparently maintaining a nativelike hydrogen bond with the D47 carboxylate group even though the protein is approximately 90% unfolded (Figure 5B). The implication is that this short-range (i, i + 2) interaction, located in the $\beta3-\beta4$ hairpin, forms early in the folding of protein G. These pH titration results are consistent with hydrogen exchange measurements (Orban et al., 1995) and peptide fragment studies (Blanco et al., 1994; Blanco & Serrano, 1995) which indicate that the most stable region in the protein is the $\beta3-\beta4$ hairpin. In addition, ^{15}N relaxation measurements on urea-denatured B1 at low pH show that the $\beta3-\beta4$ region is one of the less mobile parts of the polypeptide chain (Frank et al., 1995). Furthermore, kinetic pulse-labeling experiments indicate that slow exchange NHs in the $\beta3-\beta4$ hairpin have higher protection factors than other residues in the β-sheet (Kuszewski et al., 1994).

Our results suggest that the H-bonding interaction between the Y45 and D47 side chains may be quite strong. This may not be surprising since H-bonds between oxygens are known to be among the strongest in proteins, particularly when tyrosine hydroxyl groups are involved (Schulz & Schirmer, 1979). We are further investigating the possibility of anomalously strong H-bonds by monitoring fractionation factors in protein G (Loh & Markley, 1994).

REFERENCES

Achari, A., Hale, S. P., Howard, A. J., Clore, G. M., Gronenborn, A. M., Hardman, K. D., & Whitlow, M. (1992) *Biochemistry 31*, 10449−10457.

Alexander, P., Fahnestock, S., Lee, T., Orban, J., & Bryan, P. (1992a) *Biochemistry 31*, 3597−3603.

Alexander, P., Orban, J., & Bryan, P. (1992b) *Biochemistry 31*, 7243−7248.

Anderson, D. E., Lu, J., McIntosh, L., & Dahlquist, F. W. (1993) in *NMR of Proteins* (Clore, G. M., & Gronenborn, A. M., Eds.), pp 258−304, CRC Press, Boca Raton, FL.

Antosiewicz, J., McCammon, J. A., & Gilson, M. K. (1994) *J. Mol. Biol. 238*, 415−436.

Antosiewicz, J., McCammon, J. A., & Gilson, M. K. (1996) *Biochemistry 35*, 7819−7833.

Bai, Y., Milne, J. S., Mayne, L., & Englander, S. W. (1993) *Proteins: Struct., Funct., Genet. 17*, 75−86.

Bartik, K., Redfield, C., & Dobson, C. M. (1994) *Biophys. J. 66*, 1180−1184.

Bashford, D., & Karplus, M. (1990) *Biochemistry 29*, 10219−10225.

Bashford, D., Case, D. A., Dalvit, C., Tennant, L., & Wright, P. E. (1993) *Biochemistry 32*, 8045−8056.

Bax, A. (1989) *Methods Enzymol. 176*, 151−168.

Bax, A., Ikura, M., Kay, L. E., Torchia, D. A., & Tschudin, R. (1990) *J. Magn. Reson. 86*, 304−318.

Bernstein, F. C., Koetzle, T. F., Williams, T. F., Meyer, G. J. B., Jr., Brice, M. D., Rodgers, J. R., Kennard, O., Shimanouchi, T., & Tasumi, M. (1977) *J. Mol. Biol. 112*, 535−542.

Blanco, F. J., & Serrano, L. (1995) *Eur. J. Biochem. 230*, 634−649.

Blanco, F. J., Rivas, G., & Serrano, L. (1994) *Nature Struct. Biol. 1*, 584−590.

Bodenhausen, G., & Ruben, D. J. (1980) *Chem. Phys. Lett. 69*, 185−189.

Braunschweiler, L., & Ernst, R. R. (1983) *J. Magn. Reson. 53*, 521−528.

Brooks, B. R., Bruccoleri, R. E., Olafson, B. D., States, D. J., Swaminathan, S., & Karplus, M. (1983) *J. Comput. Chem. 4*, 187−217.

Brunger, A. T., & Karplus, M. (1988) *Proteins: Struct., Funct., Genet. 4*, 148−156.

Bundi, A., & Wuthrich, K. (1979) *Biopolymers 18*, 299−311.

Clore, G. M., & Gronenborn, A. M. (1992) *J. Mol. Biol. 223*, 853−856.

Cohen, J. S., Griffin, J. H., & Schechter, A. N. (1973) *J. Biol. Chem. 248*, 4305−4310.

Davis, M. E., Madura, J. D., Luty, B. A., & McCammon, J. A. (1991) *Comput. Phys. Commun. 62*, 187−197.

DeMarco, A. (1977) *J. Magn. Reson. 26*, 527−528.

Derrick, J. P., & Wigley, D. B. (1994) *J. Mol. Biol. 243*, 906−918.

Ebina, S., & Wuthrich, K. (1984) *J. Mol. Biol. 179*, 283−288.

Fahnestock, S. R., Alexander, P., Nagle, J., & Filpula, D. (1986) *J. Bacteriol. 167*, 870−880.

Forman-Kay, J. D., Clore, G. M., & Gronenborn, A. M. (1992) *Biochemistry 31*, 3442−3452.

Frank, M. K., Clore, G. M., & Gronenborn, A. M. (1995) *Protein Sci. 4*, 2605−2615.

Gallagher, T., Alexander, P., Bryan, P., & Gilliland, G. L. (1994) *Biochemistry 33*, 4721−4729.

Gilson, M. K. (1993) *Proteins: Struct., Funct. Genet. 15*, 266−282.

Gilson, M. K. (1997) in *Computer Simulations of Biomolecular Systems* (Wilkinson, T., & Weiner, P., Eds.) Escom, The Netherlands (in press).

Gilson, M. K., & Honig, B. (1988) *Proteins: Struct., Funct., Genet. 4*, 7−18.

Gilson, M. K., Rashin, A. A., Fine, R., & Honig, B. (1985) *J. Mol. Biol. 183*, 503−516.

Gilson, M. K., Sharp, K. A., & Honig, B. H. (1988) *J. Comput. Chem. 9*, 327−335.

Glasoe, P. F., & Long, F. A. (1960) *J. Phys. Chem. 64*, 188−193.

Gronenborn, A. M., Filpula, D. R., Essig, N. Z., Achari, A., Whitlow, M., Wingfield, P. T., & Clore, G. M. (1991) *Science 253*, 657−661.

Honig, B., & Hubbell, W. (1984) *Proc. Natl. Acad. Sci. U.S.A. 81*, 5412−5416.

Honig, B., Sharp, K., & Yang, A.-S. (1993) *J. Phys. Chem 97*, 1101−1109.

Huyghues-Despointes, B. M. P., Klingler, T. M., & Baldwin, R. L. (1995) *Biochemistry 34*, 13267−13271.

Jardetzky, O., & Roberts, G. C. K. (1981) *NMR in Molecular Biology*, Academic Press, New York.

Jeng, M.-F., & Dyson, H. J. (1996) *Biochemistry 35*, 1−6.

Jeng, M.-F., Holmgren, A., & Dyson, H. J. (1995) *Biochemistry 34*, 10101−10105.

Jorgensen, W. L., & Tirado-Rives, J. (1988) *J. Am. Chem. Soc. 110*, 1657−1666.
Klapper, I., Hagstrom, R., Fine, R., Sharp, K., & Honig, B. (1986) *Proteins: Struct., Funct., Genet. 1*, 47−79.
Kraulis, P. J. (1991) *J. Appl. Crystallogr. 24*, 946−950.
Kuszewski, J., Clore, G. M., & Gronenborn, A. M. (1994) *Protein Sci. 3*, 1945−1952.
Lian, L.-Y., Derrick, J. P., Sutcliffe, M. J., Yang, J. C., & Roberts, G. C. K. (1992) *J. Mol. Biol. 228*, 1219−1234.
Loh, S. N., & Markley, J. L. (1994) *Biochemistry 33*, 1029−1036.
Madura, J. D., Davis, M. E., Gilson, M. K., Wade, R. C., Luty, B. A., & McCammon, J. A. (1994) *Rev. Comput. Chem. 5*, 229−267.
Marion, D., & Wuthrich, K. (1983) *Biochem. Biophys. Res. Commun. 113*, 967−974.
Marion, D., Ikura, M., Tschudin, R., & Bax, A. (1989) *J. Magn. Reson. 85*, 393−399.
Myhre, E. B., & Kronvall, G. (1977) *Infect. Immun. 17*, 475−482.
Norwood, T. J., Boyd, J., Heritage, J. E., Soffe, N., & Campbell, I. D. (1990) *J. Magn. Reson. 87*, 488−501.
Orban, J., Alexander, P., & Bryan, P. (1992) *Biochemistry 31*, 3604−3611.
Orban, J., Alexander, P., & Bryan, P. (1994) *Biochemistry 33*, 5702−5710.
Orban, J., Alexander, P., Bryan, P., & Khare, D. (1995) *Biochemistry 34*, 15291−15300.
Patel, D. J., Canuel, L. L., Woodward, C., & Bovey, F. A. (1975) *Biopolymers 14*, 959−974.
Perrin, C. L., & Arrhenius, G. M. L. (1982) *J. Am. Chem. Soc. 104*, 6693−6696.
Qin, J., Clore, G. M., & Gronenborn, A. M. (1996) *Biochemistry 35*, 7−13.
Redfield, A. G., & Waelder, S. (1979) *J. Am. Chem. Soc. 101*, 6151−6162.
Reis, K. J., Ayoub, E. M., & Boyle, M. D. P. (1984) *J. Immunol. 132*, 3098−3102.
Rucker, S. P., & Shaka, A. J. (1989) *Mol. Phys. 68*, 509−517.
Schaller, W., & Robertson, A. D. (1995) *Biochemistry 34*, 4714−4723.
Schellman, J. A. (1975) *Biopolymers 14*, 999−1018.
Schulz, G. E., & Schirmer, R. H. (1979) *Principles of Protein Structure*, pp 33−36, Springer-Verlag, New York.
Shaka, A. J., Barker, P. B., & Freeman, R. (1985) *J. Magn. Reson. 64*, 547−552.
Shaka, A. J., Lee, C. J., & Pines, A. (1988) *J. Magn. Reson. 77*, 274−293.
States, D. J., & Karplus, M. (1987) *J. Mol. Biol. 197*, 131−140.
Szyperski, T., Antuch, W., Schick, M., Betz, A., Stone, S. R., & Wuthrich, K. (1994) *Biochemistry 33*, 9303−9310.
Takahashi, T., Nakamura, H., & Wada, A. (1992) *Biopolymers 32*, 897−909.
Tanford, C., & Kirkwood, J. G. (1957) *J. Am. Chem. Soc. 79*, 5333−5339.
Tashiro, M., & Montelione, G. T. (1995) *Curr. Opin. Struct. Biol. 5*, 471−481.
Taylor, R., Kennard, O., & Versichel, W. (1984) *Acta Crystallogr. B 40*, 280−288.
Wagner, G. (1990) *Prog. NMR Spectrosc. 22*, 101−139.
Wang, Y.-X., Freedberg, D. I., Yamazaki, T., Wingfield, P. T., Stahl, S. J., Kaufman, J. D., Kiso, Y., & Torchia, D. A. (1996) *Biochemistry 35*, 9945−9950.
Warwicker, J., & Watson, H. C. (1982) *J. Mol. Biol. 157*, 671−679.
Wilson, N. A., Barbar, E., Fuchs, J. A., & Woodward, C. (1995) *Biochemistry 34*, 8931−8939.

BI9630927